Transport in Porous Media **29:** 309–321, 1997.

Non-Darcy Free Convection Along a Horizontal Heated Surface

M. A. HOSSAIN[1] and D. A. S. REES[2]
[1]*Department of Mathematics, University of Dhaka, Dhaka 1000, Bangladesh*
e-mail: ahossain@triton.kaifnet.com
[2]*Department of Mechanical Engineering, University of Bath, Bath BA7 2AY, U.K.*

(Received: 30 September 1996; in final form: 5 August 1997)

Abstract. In this paper we analyse how the presence of inertia (Forchheimer form-drag) affects the steady free convective boundary layer flow over an upward-facing horizontal surface embedded in a porous medium. The surface temperature is assumed to display a power-law variation, x^n, with distance from the leading edge, x. It is shown that there are three distinct cases to consider: $n < 0.5$, $n = 0.5$ and $0.5 < n \leqslant 2$. In the first case inertia dominates the flow near the leading edge, but its effect wanes downstream. The boundary layer is self-similar in the second case with the resulting profiles being dependent on the strength of the inertia effect. In the third case, inertia effects grow with increasing distance from the leading edge, and the boundary-layer thickness is greater than when inertia is absent.

Key words: Non-Darcy, free convection, horizontal surface, fluid inertia.

Nomenclature

d	microscopic length scale
$f, F, \mathcal{F}$	reduced stream function
$\bar{g}$	acceleration due to gravity
$g, G, \mathcal{G}$	scaled temperature
Gr	Darcy–Grashof number defined in Equation (10b)
K	permeability
$\tilde{K}$	inertial parameter
n	power-law index
Q	fluid flux velocity
Ra	Darcy–Rayleigh number defined in Equation (10a)
T	temperature
u	fluid flux velocity component in the x direction
v	fluid flux velocity component in the y direction
x	Cartesian coordinate in the streamwise direction
X	scaled streamwise coordinate
y	Cartesian coordinate in the cross-stream direction

Greek Symbols

α	nondimensional inertia parameter
β	coefficient of thermal expansion
η	pseudo-similarity variable
ζ	pseudo-similarity variable
χ	pseudo-similarity variable
ϵ	porosity
ξ	scaled streamwise coordinate
θ	dimensionless temperature
κ	effective thermal diffusivity
ρ	fluid density
μ	viscosity
ψ	stream function

1. Introduction

In this paper we investigate the detailed effect of fluid inertia, as modelled by the quadratic Forchheimer terms, on the free convective boundary-layer flow induced by a

horizontal surface with a power-law surface temperature. As such, this is an extension of a recent paper by Rees (1996) who considered only the uniform surface temperature case. Free convection boundary layers occur frequently in porous media, and the topic has applications in in geophysics, thermal insulation engineering and heat storage systems. As was pointed out by Rees (1996), the horizontal free convection boundary layer induced by a flat surface with a uniform temperature is fairly weak, and therefore the effects of inertia are typically only manifest when a higher-order boundary-layer theory is undertaken, see Riley and Rees (1985). However, Rees (1996) showed that it is possible to have inertia modify the leading order boundary-layer flow when either (i) a suitably defined inertia parameter is sufficiently large, or (ii) when distances fairly close to the leading edge are considered. The aim of the present paper is to investigate how a nonuniformly heated surface modifies these qualitative phenomena.

Free convection from a horizontal surface was first studied by Cheng and Chang (1976) who investigated Darcy flow. This work was extended to higher order by Riley and Rees (1985) who also considered the detailed effects of inertia, and by Chang and Cheng (1983). Subsequent work on this problem has centred on mixed convection (e.g. Kumari *et al.*, 1990) suction/injection of fluid at the surface (e.g. Minkowycz *et al.*, 1985; Lai and Kulacki, 1990) and aspects of the stability of the flow (e.g. Hsu *et al.*, 1978; Jang and Chang, 1988; Storesletten and Rees, 1997; Rees, 1997a). However, we shall attend to the seemingly straightforward case where inertia is present in the free convective boundary layer, as a good understanding of the role of inertia on the development of the flow and its associated rate of heat transfer is still lacking.

In general, the governing boundary-layer equations are not self-similar and therefore we employ the Keller-box method to integrate the resulting parabolic equations. It is found that three distinct cases arise depending on the value of the power-law exponent, n. In the first case, where $n < 0.5$, inertia dominates near the leading edge, but its effect diminishes as the leading edge recedes. The precise opposite is true when $n > 0.5$, in that inertia is absent at the leading edge, but its effect becomes stronger further downstream. When $n = 0.5$ there is a transition between these two behaviours, and the flow is self-similar in this case.

2. Governing Equations and the Boundary-Layer Approximation

We consider a horizontal surface which is embedded in a homogeneous fluid-saturated porous medium. The surface is held at the temperature, $T_w = T_\infty + A(x^*)^n$, whilst the ambient temperature of the medium is T_∞. We assume that $T_w > T_\infty$ (i.e. that $A > 0$) and examine the resulting two-dimensional flow induced by buoyancy forces in the medium along the surface. The governing dimensional equations are

$$u^*_{x^*} + v^*_{y^*} = 0, \tag{1}$$

$$\left(1 + \frac{\tilde{K}}{\mu}|\mathbf{u}^*|\right) u^* = -\frac{K}{\mu} p^*_{x^*}, \tag{2}$$

$$\left(1+\frac{\tilde{K}}{\mu}|\mathbf{u}^*|\right)v^* = -\frac{K}{\mu}(p^*_{y^*} - \rho g\beta(T-T_\infty)), \tag{3}$$

$$u^*T_{x^*} + v^*T_{y^*} = \kappa(T_{x^*x^*} + T_{y^*y^*}), \tag{4}$$

(see Riley and Rees, 1985) and Darcy's law is recovered when $\tilde{K} = 0$. In Equations (1)–(4) x^* and y^* are the Cartesian coordinates along and perpendicular to the heated plate, respectively, u^* and v^* are the respective fluid velocity fluxes, p is the dynamic pressure and T is the temperature. Here, K is the permeability of the porous medium, $\tilde{K}$ is a material parameter measuring the inertial impedance of the matrix, g is the acceleration due to gravity, ρ the fluid density, μ the dynamic viscosity, β the coefficient of cubical expansion of the fluid and κ the effective thermal diffusivity of the saturated medium. Ergun's (1952) relations,

$$K = \frac{d^2\varepsilon^3}{150(1-\varepsilon)^2}, \qquad \tilde{K} = \frac{1.75d}{150(1-\varepsilon)}, \tag{5}$$

illustrate how K and $\tilde{K}$ vary with ε, the porosity, and d, the characteristic pore or particle diameter. Clearly, when $\varepsilon \sim 1$ then $\tilde{K}$ is large and the nonlinear term is important. Equations (1)–(4) are nondimensionalised using the substitutions,

$$(x^*, y^*) = l(x, y), \qquad (u^*, v^*) = \frac{\kappa}{l}(u, v), \tag{6a,b}$$

$$p^* = \frac{\kappa\mu}{K}p, \qquad T = T_\infty + Al^n\theta, \tag{6c,d}$$

where l is a macroscopic lengthscale. When the two-dimensional stream function is introduced using

$$(u, v) = (\psi_y, -\psi_x) \tag{7}$$

then we obtain the equations,

$$\begin{aligned}&(1 + \mathrm{Gr}\,Q/\mathrm{Ra})\nabla^2\psi + (\mathrm{Gr}/Q\mathrm{Ra})\times\\ &\quad\times(\psi_x^2\psi_{xx} + 2\psi_x\psi_y\psi_{xy} + \psi_y^2\psi_{yy}) = -\mathrm{Ra}\,\theta_x,\end{aligned} \tag{8}$$

$$\nabla^2\theta = \psi_y\theta_x - \psi_x\theta_y. \tag{9}$$

The Darcy–Rayleigh number, Ra, and the Darcy–Grashof number, Gr, are given by

$$\mathrm{Ra} = \frac{\rho g\beta(T_w - T_\infty)lK}{\kappa\mu}, \qquad \mathrm{Gr} = \frac{\rho K\tilde{K}g\beta(T_w - T_\infty)}{\mu^2}, \tag{10a,b}$$

and Q is a fluid flux given by

$$Q^2 = \psi_x^2 + \psi_y^2. \tag{11}$$

If we assume that $x = \mathrm{O}(1)$ as $\mathrm{Ra} \to \infty$, then the boundary-layer approximation is valid when $y \ll 1$. Subject to this approximation, Equations (8) and (9) reduce to

$$(1 + 2|\psi_y|\mathrm{Gr}\,\mathrm{Ra}^{-1})\psi_{yy} = -\mathrm{Ra}\theta_x, \tag{12}$$

$$\theta_{yy} = \psi_y\theta_x - \psi_x\theta_y, \tag{13}$$

and the boundary conditions are,

$$\psi = 0, \quad \theta = x^n \qquad \text{on} \quad y = 0, \tag{14}$$

$$\psi_y \to 0, \quad \theta \to 0 \qquad \text{as} \quad y \to \infty. \tag{15}$$

Following Rees (1996) we introduce the following scalings,

$$\psi = \mathrm{Ra}^{1/3}\hat{\psi}, \quad y = \mathrm{Ra}^{-1/3}\hat{y}, \quad x = \hat{x}, \quad \text{and} \quad \mathrm{Gr} = \alpha\,\mathrm{Ra}^{1/3} \tag{16}$$

into Equations (12) and (13). Here, α is a constant which measures the strength of the fluid inertia. Hence, ψ and θ satisfy the following equations:

$$(1 + 2\alpha\hat{\psi}_{\hat{y}})\hat{\psi}_{\hat{y}\hat{y}} = -\theta_{\hat{x}}, \tag{17}$$

$$\theta_{\hat{y}\hat{y}} = \hat{\psi}_{\hat{y}}\theta_{\hat{x}} - \hat{\psi}_{\hat{x}}\theta_{\hat{y}}, \tag{18}$$

where the modulus sign which is present in Equation (12) has been dropped in Equation (17) since the function $\hat{\psi}_{\hat{y}}$ is always positive. The constant, α, can be scaled out of the equations by introducing the transformation,

$$\hat{\psi} = \alpha^{\frac{1+n}{1-2n}}\bar{\psi}, \qquad \hat{x} = \alpha^{\frac{2n+3}{1-2n}}\bar{x}, \qquad \hat{y} = \alpha^{\frac{2-n}{1-2n}}\bar{y}, \qquad \hat{\theta} = \alpha^{\frac{(2n+3)n}{1-2n}}\bar{\theta}. \tag{19}$$

Equations (17) and (18) now become,

$$(1 + 2\bar{\psi}_{\bar{y}})\bar{\psi}_{\bar{y}\bar{y}} = -\bar{\theta}_{\bar{x}}, \tag{20}$$

$$\bar{\theta}_{\bar{y}\bar{y}} = \bar{\psi}_{\bar{y}}\bar{\theta}_{\bar{x}} - \bar{\psi}_{\bar{x}}\bar{\theta}_{\bar{y}}. \tag{21}$$

It is important to note at this point that the transformations given by Equation (19) are invalid when $n = 0.5$, and therefore this specific case merits seperate attention. It is also necessary to state that the equivalent transformation in Rees (1996) is in error, and should be replaced by the present Equation (19) with $n = 0$. The approriate similarity variables for further analysis now depend on the precise value of n. Thus the boundary-layer analyses are contained in the next three sections, and correspond, respectively, to $0 \leqslant n < 0.5$, $n = 0.5$ and $0.5 < n \leqslant 2$.

3. Boundary Layer Flow for $0 \leqslant n < 0.5$

At the outset we shall regard the presence of inertia as a perturbation to Darcy flow, and therefore we introduce the transformation,

$$\bar{\psi} = \bar{x}^{(1+n)/3} f(\xi, \eta), \qquad \bar{\theta} = \bar{x}^n \theta(\xi, \eta), \tag{22}$$

$$\xi = \bar{x}^{(1-2n)/3}, \qquad \eta = \bar{y}/\bar{x}^{(2-n)/3}, \tag{23}$$

which is the appropriate one for Darcy flow. Equations (20) and (21) reduce to the form,

$$(1 + 2\xi^{-1} f_\eta) f_{\eta\eta} = \left(\frac{2-n}{3}\right) \eta g_\eta - ng - \left(\frac{1-2n}{3}\right) \xi g_\xi, \tag{24}$$

$$g_{\eta\eta} + \left(\frac{1+n}{3}\right) f g_\eta - n f_\eta g = \left(\frac{1-2n}{3}\right) \xi (f_\eta g_\xi - f_\xi g_\eta), \tag{25}$$

and the boundary conditions become

$$f = 0, \quad \theta = 1, \quad \text{on} \quad \eta = 0 \quad \text{and} \quad f_\eta, \theta \to 0 \qquad \text{as} \ \eta \to \infty. \tag{26}$$

Given the presence of the ξ^{-1} term in Equation (24) we see that inertial effects decay as ξ becomes large. But when ξ is close to zero inertial effects dominate and we must use the different transformation:

$$\bar{\psi} = \bar{x}^{(2+n)/5} F(X, \zeta), \qquad \bar{\theta} = \bar{x}^n \theta(X, \zeta), \tag{27}$$

$$X = \bar{x}^{(1-2n)/5}, \qquad \zeta = \bar{y}/\bar{x}^{(3-n)/5}. \tag{28}$$

Equations (20) and (21) become

$$(X + 2F_\zeta) F_{\zeta\zeta} = \left(\frac{3-n}{5}\right) \zeta G_\zeta - nG - \left(\frac{1-2n}{5}\right) X G_X, \tag{29}$$

$$G_{\zeta\zeta} + \left(\frac{2+n}{5}\right) F G_\zeta - n F_\zeta G = \left(\frac{1-2n}{5}\right) X (F_\zeta G_X - F_X G_\zeta), \tag{30}$$

and the boundary conditions are

$$F = 0, \quad G = 1, \quad \text{on} \quad \zeta = 0 \quad \text{and} \quad F_\zeta, G \to 0 \quad \text{as} \ \zeta \to \infty. \tag{31}$$

Equations (24) and (25) and Equations (29) and (30) were solved using the Keller-box method (see Keller and Cebeci, 1971; Cebeci and Bradshaw, 1984) a very well-established technique for studying nonsimilar boundary layer flows. The particular implementation used here follows recent papers (Rees, 1997b,c) which uses a numerical differentiation procedure to generate the Jacobian matrix forming the central Newton–Raphson iteration scheme. Such an implementation, though slightly slower than when the Jacobian is defined explicitly within the code, allows a much more rapid code development, and reduces the possibility of coding errors. For the present problem, Equations (29) and (30) were solved in the range, $0 \leqslant X \leqslant 1$ (equivalent to $0 \leqslant \bar{x} \leqslant 1$), and Equations (24) and (25) from $\xi = 1$ ($\bar{x} = 1$) onwards. A nonuniform η or ζ grid with 67 points lying between 0 and 40 was used, with grid points concentrated near the heated surface where variations are largest. Generally, convergence

of the Newton–Raphson iteration scheme at each streamwise station occurred on or before the 4th iteration, and this is based on a maximum pointwise correction of 10^{-8} for convergence. However, the solution procedure at $X = 0$ required special treatment as the coefficient of the highest derivative term in Equation (24) becomes exponentially small as ζ increases. Thus a satisfactory approach to the numerical solution at $X = 0$ was obtained by iterating with under-relaxation in order that numerical values of F_ζ remain positive over the whole range of integration for all iterates.

The inertia-dominated profiles for $F(\zeta)$ and $G(\zeta)$ at $X = 0$ thus obtained are depicted in Figures 1a and 1b for various values of n. For reference we also show, in Figure 2, how the scaled slip velocity, $F_\zeta(\zeta = 0)$, and rate of heat transfer, $G_\zeta(\zeta = 0)$, vary with n. It is necessary to note that Equation (30) with $n = 0$ does not agree with the uniform temperature analysis of Rees (1996) which is in error. Thus, when $n = 0$, we have $G_\zeta(\zeta = 0) = -0.4606$, and $F_\zeta(\zeta = 0) = 0.9279$, which correct the values quoted in Equation (39) of Rees (1996).

Figure 3 displays local rates of heat transfer at the heated surface as functions of X for different values of the power-law exponent, n. These are presented in two forms:

$$\text{(i)} \quad G_\zeta \ \text{ for } \ X \leqslant 1 \ \text{ and } \ \xi^{-1/5} g_\eta \ \text{ for } \ \xi \geqslant 1, \ \text{ and} \tag{32a}$$

$$\text{(ii)} \quad X^{1/3} G_\zeta \ \text{ for } \ X \leqslant 1 \ \text{ and } \ g_\eta \ \text{ for } \ \xi \geqslant 1. \tag{32b}$$

The form given in Equation (32a) allows the behaviour of the heat transfer in the inertia-dominated regime to be seen clearly, whereas Equation (32b) shows well the approach towards the Darcy-flow regime at large distances from the leading edge. In both cases, these functions are plotted against X for convenience of presentation, and we note that $X = \xi^{5/3}$. Figure 3 indicates that Darcy flow is quite quickly established as X increases.

4. Boundary-Layer Flow for $n = 0.5$

Unlike the first case described above, it is not possible to scale α out of the governing boundary-layer equations when $n = 0.5$. The physical reason for this is that the induced streamwise velocity when $n = 0.5$ does not vary with x, and therefore inertia may be either strong or weak. In this regard the situation is exactly like the thermal boundary layer induced by a vertical surface held at uniform temperature (Riley and Rees, 1985). Indeed, the flow is self-similar in this case, and the substitution of

$$\psi = \hat{x}^{1/2} f(\eta), \qquad \theta = \hat{x}^{1/2} g(\eta), \qquad \eta = \hat{y}/\hat{x}^{1/2}, \tag{33}$$

into Equations (17) and (18) yields the equations,

$$(1 + 2\alpha f') f'' = \tfrac{1}{2}(\eta g' - g), \tag{34}$$

$$g'' + \tfrac{1}{2}(f g' - f' g) = 0. \tag{35}$$

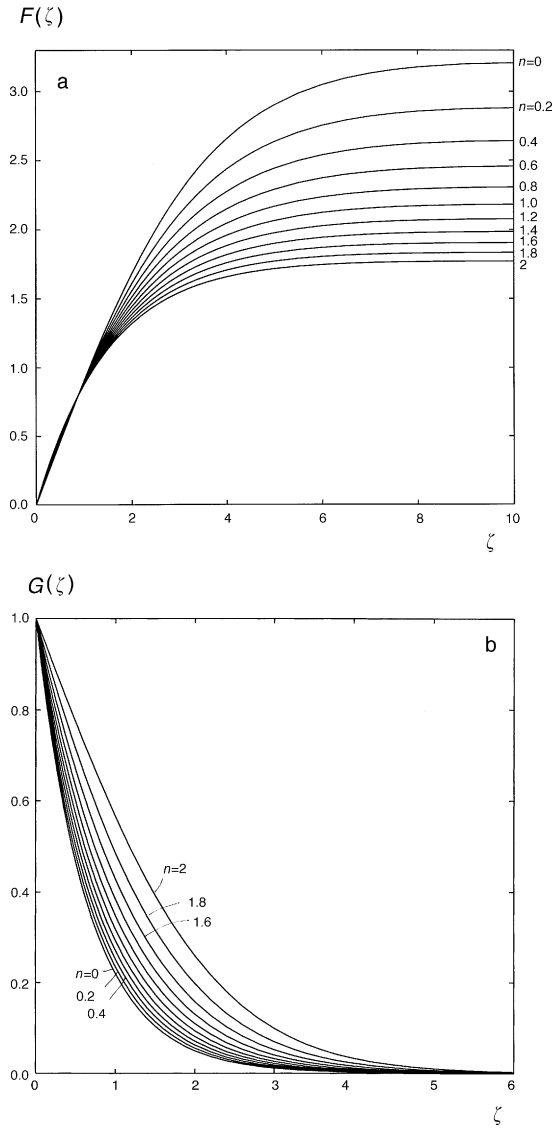

Figure 1. The inertia-dominated profiles of (a) $F(\zeta)$ and (b) $G(\zeta)$ for various values of the power-law exponent, n. These form the self-similar profiles corresponding to the solution of (29) and (30) at $X = 0$ for $n \leqslant 0.5$, and the solution of Equations (47) and (48) as $X \to \infty$ for $n \geqslant 0.5$.

These ordinary differential equations have been solved using a suitably modified version of the present Keller-box code where α in Equation (34) is treated as the marching variable in order to perform a parameter sweep with ease. The values of $f'(0)$ and $g'(0)$ as α increases from zero are displayed in Figure 4 where we see that both quantities decay as α increases. This is related to the fact that inertia serves

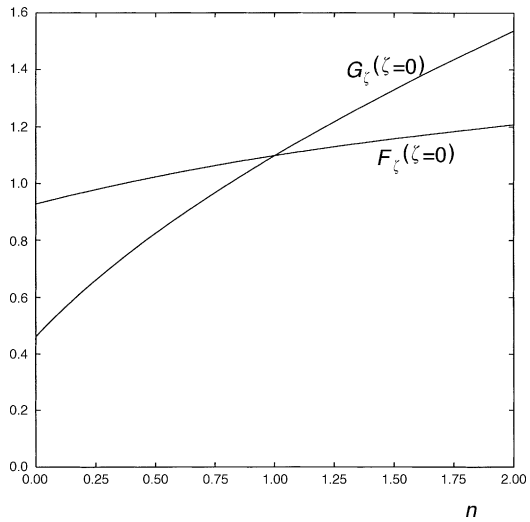

Figure 2. Variation of the slip velocity, $F_\zeta(\zeta = 0)$, and rate of heat transfer, $G_\zeta(\zeta = 0)$, at $X = 0$ as functions of n.

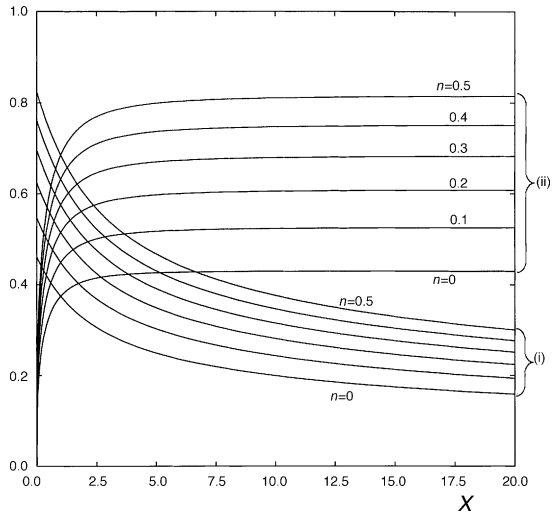

Figure 3. Local rate of heat transfer as a function of X for various values of n. The curve marked (i) corresponds to the definition given in Equation (32a), and (ii) to that in Equation (32b).

to thicken the boundary layer due to the increased effectiveness of conduction from the heated surface which is caused by the decreased advection of heat downstream. Selected numerical values are given below in Table I.

It is possible to perform a straightforward asymptotic analysis of the solutions of Equations (34) and (35) which is valid to leading order for large values of α. The

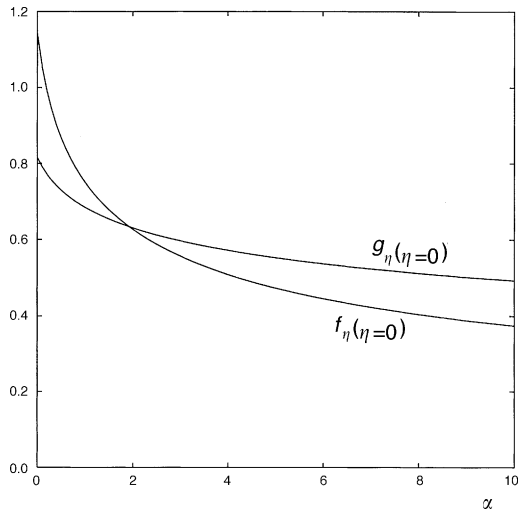

Figure 4. Variation of the slip velocity, $f_\eta(\eta = 0)$, and rate of heat transfer, $g_\eta(\eta = 0)$, for $n = 0.5$ as functions of α. Some numerical and asymptotic values are also presented in Table I.

transformation

$$f = \alpha^{-1/5}\mathcal{F}(\chi), \qquad g = \mathcal{G}(\chi), \qquad \eta = \alpha^{1/5}\chi, \tag{36}$$

upon introduction into Equations (34) and (35) yields

$$\mathcal{F}'\mathcal{F}'' = \tfrac{1}{2}(\chi\mathcal{G}' - \mathcal{G}), \tag{37}$$

$$\mathcal{G}'' + \tfrac{1}{2}(\mathcal{F}\mathcal{G}' - \mathcal{F}'\mathcal{G}) = 0. \tag{38}$$

Another modification to the Keller-box code allows a relatively easy solution of these equations. Using interval halving and Richardson Extrapolation based on the fact that discretisation errors are given in terms of a power series composed of even powers of the steplength, we find that

$$\mathcal{F}'(0) = 1.0231 \quad \text{and} \quad \mathcal{G}'(0) = -0.8239. \tag{39}$$

Hence, we obtain

$$f'(0) \sim 1.0231\alpha^{-2/5} \quad \text{and} \quad g'(0) \sim -0.8239\alpha^{-1/5}, \tag{40}$$

as the limiting behaviour as α becomes large. These values compare very favourably with the exact values at $\alpha = 100$, as may be seen in Table I.

5. Boundary-Layer Flow for $0.5 < n \leqslant 2$

In this section we consider larger values of n and treat $n = 2$ as the upper bound because the boundary layer attains a constant thickness in the Darcy-flow regime for this case.

Table I. Values of $f'(0)$ and $-g'(0)$ for selected values of α together with the respective asymptotic values given by Equation (40).

α	$f'(0)$	$\alpha^{-2/5}\mathcal{F}'(0)$	$-g'(0)$	$\alpha^{-1/5}\mathcal{G}'(0)$
0.0	1.1411		0.8165	
0.1	1.0560		0.7921	
0.2	0.9931		0.7726	
0.4	0.9029		0.7424	
0.6	0.8391		0.7192	
0.8	0.7903		0.7005	
1.0	0.7510		0.6848	
2.0	0.6271		0.6307	
3.0	0.5567		0.5967	
4.0	0.5090		0.5720	
5.0	0.4736		0.5527	
6.0	0.4459		0.5370	
7.0	0.4233		0.5237	
8.0	0.4044		0.5123	
9.0	0.3883		0.5024	
10.0	0.3743	0.4073	0.4935	0.5198
15.0	0.3240	0.3463	0.4600	0.4794
20.0	0.2918	0.3087	0.4371	0.4526
30.0	0.2511	0.2625	0.4060	0.4173
40.0	0.2253	0.2339	0.3850	0.3940
50.0	0.2071	0.2091	0.3692	0.3768
75.0	0.1773	0.1819	0.3419	0.3474
100.0	0.1587	0.1621	0.3236	0.3280

With such large values of n the buoyancy-induced motion near the leading edge is very weak indeed, and therefore Darcy flow might be expected. Motion then becomes stronger as $\bar{x}$ increases and inertial effects are felt increasingly. Thus the qualitative nature of the flow is precisely opposite to what it is when $n < 0.5$. The same pseudo-similarity variables (η and ζ) may be used, but they now apply on 'the other side' of $\bar{x} = 1$. Thus we use

$$\bar{\psi} = \bar{x}^{(2+n)/5} F(X, \zeta), \qquad \bar{\theta} = \bar{x}^n G(X, \zeta), \tag{41}$$

$$X = \bar{x}^{(2n-1)/5}, \qquad \zeta = \bar{y}/\bar{x}^{(3-n)/5}. \tag{42}$$

when $\bar{x} \geqslant 1$, and

$$\bar{\psi} = \bar{x}^{(1+n)/3} f(\xi, \eta), \qquad \bar{\theta} = \bar{x}^n g(\xi, \eta), \tag{43}$$

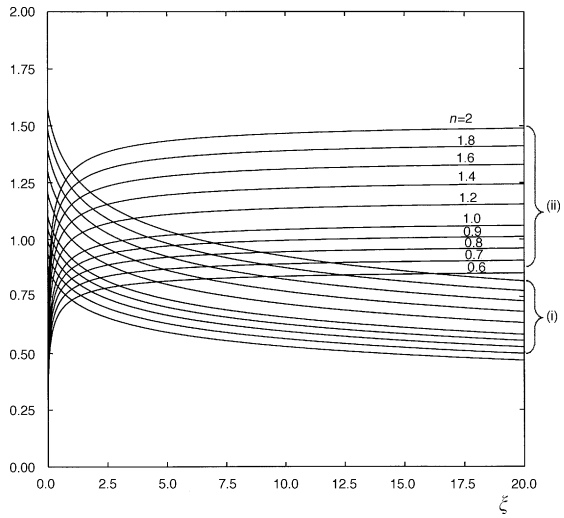

Figure 5. Local rate of heat transfer as a function of ξ for various values of n. The curve marked (i) corresponds to the definition given in Equation (49a), and (ii) to that in Equation (49b).

$$\xi = \bar{x}^{(2n-1)/3}, \qquad \eta = \bar{y}/\bar{x}^{(2-n)/3}, \tag{44}$$

when $\bar{x} \leqslant 1$. The only difference between these definitions and those of Equations (27) and (28) lies in the forms of X and ξ. The boundary layer equations are now,

$$(1 + 2\xi f_\eta) f_{\eta\eta} = \frac{2-n}{3}\eta g_\eta - ng + \frac{1-2n}{3}\xi g_\xi, \tag{45}$$

$$g_{\eta\eta} + \frac{1+n}{3} f g_\eta - n f_\eta g = \frac{2n-1}{3}\xi(f_\eta g_\xi - f_\xi g_\eta), \tag{46}$$

for $\bar{x} \leqslant 1$, and

$$(X^{-1} + 2F_\zeta) F_{\zeta\zeta} = \frac{3-n}{5}\zeta G_\zeta - nG + \frac{1-2n}{5} X G_X, \tag{47}$$

$$G_{\zeta\zeta} + \frac{2+n}{5} F G_\zeta - n F_\zeta G = \frac{2n-1}{5} X(F_\zeta G_X - F_X G_\zeta), \tag{48}$$

for $\bar{x} \geqslant 1$. These equations are solved in the same way as before, and solutions are again presented in terms of rates of heat transfer, but the definitions are now given as

(i) g_η for $\xi \leqslant 1$ and $X^{-1/3} G_\zeta$ for $X \geqslant 1$, and (49a)

(ii) $\xi^{1/5} g_\eta$ for $\xi \leqslant 1$ and G_ζ for $X \geqslant 1$; (49b)

these are displayed in Figure 5. Again, the reasons for the two forms are to see clearly both the inertia-free and inertia-dominated regimes. In this case, solutions

are plotted against ξ, for convenience. Finally, the asymptotic rates of heat transfer, $G_\zeta(\zeta = 0, X \to \infty)$, that correspond to the inertia-dominated regime, are presented in Figure 1 for various values of n.

6. Conclusions

We have investigated how the presence of inertia modifies the flow and heat transfer from a horizontal heated surface in porous media, where the surface temperature varies according to a power of x. Although inertia in the form of quadratic drag is quite weak for horizontal free convective boundary layers, there is, nevertheless, a region sufficiently close to the leading edge where inertia effects dominate (when $n < 0.5$) and where the boundary layer approximation remains valid. When $n > 0.5$, the effects of inertia grow with distance downstream as the buoyancy-induced streamwise velocity increases with distance in this case. Thus, far downstream the flow and temperature profiles, as well as the boundary-layer thickness have been changed from that where inertia is absent. In both these cases, α, the ratio of Gr and $\mathrm{Ra}^{1/3}$, may be scaled out of the mathematical problem leaving only one free parameter, n.

When $n = 0.5$ it is not possible to scale α out of the governing equations, and therefore it is necessary to study this case for various values of α. The flow is now self-similar, and an asymptotic theory for large values of α has been presented.

The main conclusion to be made is that quadratic drag modifies free convection for a horizontal surface. When $n < 0.5$ it does so close to the leading edge, but when $n > 0.5$ it will eventually do so as x increases.

References

Cebeci, T. and Bradshaw, P.: 1984, *Physical and Computational Aspects of Convective Heat Transfer*, Springer, New York.

Chang, I. D. and Cheng, P.: 1983, Matched asymptotic expansions for free convection about an impermeable horizontal surface in a porous medium, *Int. J. Heat Mass Transfer* **26**, 163–174.

Cheng, P. and Chang, I. D.: 1976, On buoyancy induced flows in a saturated porous medium adjacent to impermeable horizontal surfaces, *Int. J. Heat Mass Transfer* **19**, 1267–1272.

Ergun, S.: 1952, Fluid flow through packed columns, *Chem. Eng. Proc.* **48**, 89–94.

Hsu, C. T., Cheng, P. and Homsy, G. M.: 1978, Instability of free convection flow over a horizontal impermeable surface in a porous medium, *Int. J. Heat Mass Transfer* **21**, 1221–1228.

Jang, J. Y. and Chang, W. J.: 1988, Vortex instability of buoyancy-induced inclined boundary-layer flow in a saturated porous-medium, *Int. J. Heat Mass Transfer* **31**, 759–767.

Keller, H. B. and Cebeci, T.: 1971, Accurate numerical methods for boundary layer flows. 1. Two-dimensional flows, *Proc. Int. Conf. Numerical Methods in Fluid Dynamics*, Lecture Notes in Physics, Springer, New York.

Kumari, M., Pop, I. and Nath, G.: 1990, Non-similar boundary layer for mixed convection flow about a horizontal surface in a saturated porous medium, *Int. J. Eng. Sci.* **28**, 253–263.

Lai, F. C. and Kulacki, F. A.: 1990, The influence of surface mass flux on mixed convection over horizontal plates in saturated porous media, *Int. J. Heat Mass Transfer*, **33** 576–579.

Minkowycz, W. J. and Cheng, P. and Mialem, F.: 1985, The effect of surface mass transfer on buoyancy induced Darcian flow adjacent to a horizontal heated surface, *Int. Comm. Heat Mass Transfer* **12**, 55-65.

Rees, D. A. S.: 1996, The effect of inertia on free convection from a horizontal surface embedded in a porous medium, *Int. J. Heat Mass Transfer* **39**, 3425–3430.

Rees, D. A. S.: 1997a, Thermal boundary layer instabilities in porous media: a critical review, to appear in D. B. Ingham and I. Pop. (eds), *Transport Phenomena in Porous Media*, Springer, New York.

Rees, D. A. S.: 1997b, Free convective boundary layer flow from a heated surface in a layered porous medium, to appear in *J. Porous Media*.

Rees, D. A. S.: 1997c, Three-dimensional free convection boundary layers in porous media induced by a heated surface with spanwise temperature variations, to appear in *Trans. ASME J. Heat Transfer*.

Riley, D. S. and Rees, D. A. S.: 1985, Non-Darcy natural convection from arbitrarily inclined heated surfaces in saturated porous media, *Q. J. Mech. Appl. Math.* **38**, 277–295.

Storesletten, L. and Rees, D. A. S.: 1997, The influence of higher-order effects on the linear instability of thermal boundary layer flow in porous media, to appear in *Int. J. Heat Mass Transfer*.